Modelling and Simulation of Hypervelocity Impacts on Spacecraft in Low Earth Orbit

Rannveig M. Færgestad[1,2], Jens K. Holmen[1,3], Torodd Berstad[1,2], Tiziana Cardone[4], Kevin A. Ford[5], Tore Børvik[1,2]

[1]Structural Impact Laboratory (SIMLab), Department of Structural Engineering, NTNU – Norwegian University of Science and Technology, Trondheim, Norway
[2]Centre for Advanced Structural Analysis (SFI CASA), NTNU, Trondheim, Norway
[3]Enodo AS, Trondheim, Norway
[4]European Space Agency (ESA), ESTEC, Noordwijk, The Netherlands
[5]National Aeronautics and Space Administration (NASA), Johnson Space Center, Houston, USA

Abstract

Orbital debris is an increasing threat to current and future missions in low Earth orbit (LEO), and spacecraft shielding is vital for future space exploration efforts. Experimental hypervelocity impacts (HVI) are expensive and can only be performed at a few laboratories worldwide, making numerical simulations an essential tool in the development and design of debris shields. A debris shield is a sacrificial plate that shatters an impactor into a cloud of particles, distributing the momentum of the impactor over a large area, thus preventing it from perforating the spacecraft. In this study, HVI were modelled in LS-DYNA using a coupled finite element-discrete particle method (FEM/DES), through the ***DEFINE_ADAPTIVE_SOLID_TO_DES** keyword. The results were compared to experimental data from the literature as well as to simulations applying the smoothed particle hydrodynamics (SPH) method. First, impacts by projectiles with diameter below 1 cm and impact velocities up to 6.7 km/s were simulated to study the debris cloud after perforation of a single plate. Here, aluminium alloy AA6061-T6 was used as both the target and the projectile material. The FEM/DES method was able to predict the shape of the debris cloud as a function of impactor shape, impactor velocity and shield thickness. Then, the FEM/DES method was applied to a dual-wall Whipple shield configuration and was able to accurately describe the damage from the debris cloud on the rear wall.

1 Introduction

Providing efficient spacecraft shielding and protection from space debris is essential to ensure safe and successful operations of spacecraft and satellites. The development of low-weight effective shields has enabled the risk of critical damage to spacecraft to be reduced while also minimising the weight and volume of the design. Whipple [1] first introduced the idea of an outer sacrificial shield for spacecraft in 1947. Such Whipple shields consist of a single bumper, followed by a rear wall at a standoff distance. The function of the sacrificial shield, or bumper, is to break up the impacting particle into a cloud of vaporised, liquid, and/or solid material that expands in the space behind the bumper. The momentum and energy of the particles are then distributed over a wide area of the rear wall. The rear wall must be thick enough to withstand the blast-like loading from the debris cloud and any solid fragments remaining. The Whipple shield is more mass-effective than a single-wall shield at withstanding an impact but adds additional volume to the design. The capability of a shield to protect from projectiles impacting at hypervelocity is described by a ballistic limit equation (BLE). BLEs describe a critical projectile diameter D_C that causes shield failure, typically as a function of impact velocity, angle, density, and shape of the projectile [2]. Failure of the shield is achieved for projectile diameters greater than the critical diameter. Failure of a shield is defined as complete perforation or detached spall from the rear wall. BLEs are typically empirically fitted equations made to model complex phenomena using a simple analytical form.

Smoothed particle hydrodynamics (SPH) is the most widely used method for modelling hypervelocity impact (HVI) problems (e.g., [3], [4], [5] and [6]) because the mesh-less formulation allows for easy handling of the localised, hydrodynamic material behaviour found under such conditions. Another computational approach that can be applied to HVI problems is the discrete element method (DEM), implemented in LS-DYNA as discrete element spheres (DES). DES models a material as a collection of independent particles connected at the boundaries, where bonded particles can interact with cohesive and repulsive forces. Coupled methods try to combine the benefits of using particles (SPH or DES) to describe the localised hydrodynamic behaviour in the impact zone, with the benefit of using finite elements for the global structural response, by converting distorted elements to particles once a criterion is reached.

HVI problems are typically modelled with a non-linear Mie-Grüneisen equation of state (EOS) (e.g., [3], [5], [6], [7] and [8]) since it gives a suitable theoretical description of the pressure states in a shocked solid. The influence of the EOS in numerical models was investigated for ballistic impacts with bullets at velocities up to 7 km/s by Børvik et al. [9]. The difference between the linear and non-linear EOS was found to be minor, except for at the highest velocity where the non-linear EOS was found to be more stable. Linear EOS has the significant benefit that it does not require additional calibration, in contrast to the often complex calibration procedure behind the non-linear EOS. Investigating the effect and influence of a linear versus a non-linear EOS at hypervelocity is therefore also of strong interest.

2 Piekutowski Experiments

The numerical results presented in this study were compared to the experimental data by Piekutowski [10], where the formation and description of debris clouds by HVI were investigated and presented. Velocities up to 7.4 km/s were used in the tests, which at the time was close to the highest achievable velocities in a laboratory setting. The test data provided, among others, a thorough evaluation of the effect of target-thickness-to-projectile-diameter ratio (t/D), impact velocity and material on the debris cloud formation process. The experimental results presented in Piekutowski's report have been widely used to compare and validate models for HVI.

The experimental results in Piekutowski's report that will be considered here is the target thickness study, where the impact velocity and the projectile diameter (D) were kept constant at 6.7 km/s and 9.53 mm, respectively, while the target thickness (t) was varied from 0.246 to 4.039 mm. Radiographs from the impact test with t = 0.968 (t/D = 0.102) are shown in Figure 1. As the t/D ratio was increased at constant impact velocity, a significant expansion of the debris cloud was found, while the size of the fragments at the centre of the debris cloud decreased.

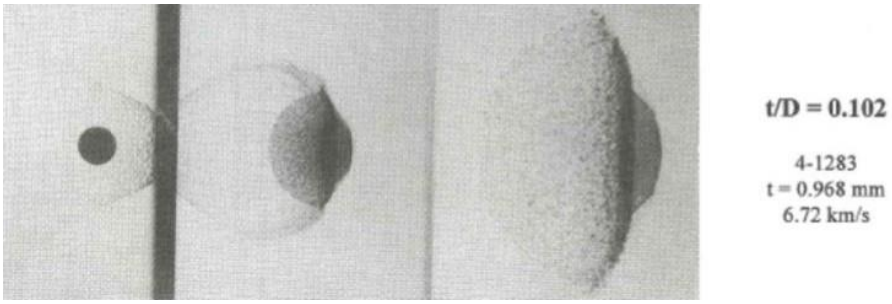

Fig.1: Radiographs from target thickness study, with t/D 0.102 at 6.72 km/s impact velocity [10].

3 Material modelling

In computational codes, the stress tensor describing the material state is usually divided into deviatoric and hydrostatic parts. The deviatoric part is related to the shear strength of the material and is described by a pressure-independent thermo-viscoplastic constitutive relation. The hydrostatic part relates the pressure, volume and internal energy of the material and is described by an EOS. The constitutive relation, EOS, and fracture criterion for HVI applied in this study are presented below.

3.1 Constitutive Relation

The modified Johnson-Cook (MJC) constitutive relation [11] [12] uses the extended Voce hardening rule to describe the hardening and a power law to describe rate sensitivity. The equivalent stress σ_{eq} is given by

$$\sigma_{\mathrm{eq}} = \big(\sigma_0 + R(p)\big)(1+\dot{p}^*)^C(1-(T^*)^m) \tag{1}$$

where

$$\dot{p}^* = \frac{\dot{p}}{\dot{p}_0}, \qquad T^* = \frac{T-T_0}{T_{\mathrm{m}}-T_0}, \qquad \Delta T = \int_0^p \chi \frac{\sigma_{\mathrm{eq}}\mathrm{d}p}{\rho C_{\mathrm{p}}}, \qquad R(p) = \sum_i Q_i(1-e^{-C_i p}) \tag{2}$$

Here, σ_0 is the yield stress, R is the hardening variable as a function of the equivalent plastic strain p, $\dot{p}$ is the equivalent plastic strain rate, $\dot{p}_0$ is a reference plastic strain rate, and C is the strain-rate sensitivity constant. Further, T^* is the homologous temperature, T is the current temperature, T_{m} is the melting

temperature and T_0 is the ambient temperature. ΔT is the increase in temperature under the assumption of adiabatic conditions at high strain rates, ρ is the material density, C_p is the specific heat capacity at constant pressure, χ is the Taylor-Quinney empirical coefficient, and Q_i and C_i are Voce hardening parameters. The material parameters for the MJC model can be determined from uniaxial tension tests conducted at strain rates and temperatures suitable for the application at hand.

3.2 Equations of State (EOS)

An EOS relates the pressure, volume, and internal energy of matter, and describes the hydrostatic behaviour of the material. A linear EOS is generally used for applications at low pressures (< 20 GPa), while a non-linear EOS is considered suitable for applications at high pressures (> 20 GPa).

Linear EOS
For low velocities and pressures, the EOS relates the pressure to the volumetric strain linearly using the bulk modulus, given as

$$P(E,\nu) = -K\varepsilon_\mathrm{v} = -\frac{E}{3(1-2\nu)}\varepsilon_\mathrm{v} \tag{3}$$

where P is the pressure, K is the bulk modulus, which is a function of Young's modulus E and Poisson's ratio ν, and ε_v is the volumetric strain. The linear EOS is therefore determined for a given material using only the two elastic material parameters.

Non-linear EOS
For higher velocities and pressures, the effects of internal energy can be significant, and the relationship between the pressure and the volumetric strain may become non-linear. The Mie-Grüneisen EOS is valid for inert solids and is widely used to describe pressure states in shocked solids [13]. The Mie-Grüneisen EOS can be expressed as

$$P(\rho,e) = P_0(1-\Gamma\eta) + \frac{\rho_0 c_0^2 \eta}{1-s\eta}\cdot\left(1-\frac{\Gamma\eta}{2}\right) + \Gamma\rho_0(e-e_0) \tag{4}$$

where P is the pressure, ρ is the density, e is the internal energy, Γ is the Grüneisen gamma, $\eta = 1 - \rho_0/\rho$, c_0 is the elastic wave speed, and s is the linear Hugoniot slope coefficient. Γ and s must be calibrated for a given material through flyer-plate impact tests or similar. Alternative formulations of the EOS also use an additional parameter, a, i.e., the first order volume correction to the Grüneisen gamma.

3.3 Failure Criterion

The Cockroft-Latham (CL) failure criterion [14] is a phenomenological ductile fracture criterion depending on the plastic strain as well as the stress triaxiality ratio and the Lode angle through the maximum principal stress. The Cockcroft-Latham failure criterion is given by

$$\omega = \frac{1}{W_\mathrm{c}}\int_0^p \max(\sigma_I, 0)\,\mathrm{d}p \tag{5}$$

where ω is the damage variable, W_c is the CL parameter representing the "plastic work" required to reach failure, and σ_I is the maximum principal stress. Fracture occurs when ω = 1. The fracture parameter W_c is the only material constant and can be determined from a uniaxial tension test.

3.4 Material Parameters

Both the projectile and target were modelled as aluminium alloy AA6061-T6. Table 1 presents the material parameters used for the MJC constitutive model and the CL failure criterion. The Voce hardening parameters utilised in this study [15] are similar to those presented in [16]. The applied material model is similar to ***MAT_107** in LS-DYNA, based on the work by Børvik et al. [12]. However, ***MAT_107** cannot be combined with a non-linear EOS, so in this study a user-defined material subroutine (UMAT) was implemented to enable combination of the MJC model and a non-linear EOS.

Table 1: Calibrated parameters for the modified Johnson-Cook constitutive model with Voce hardening [15] and the Cockroft-Latham failure criterion [16].

σ_0 [MPa]	Q_1 [MPa]	C_1 [–]	Q_2 [MPa]	C_2 [–]	W_c [MPa]
292.6	2.7	2160.7	707.6	8.94	278

Table 2 presents the bulk modulus used in the linear EOS that was defined in LS-DYNA using the ***EOS_LINEAR_POLYNOMIAL** keyword.

Table 2: Material parameter for the linear EOS.

K [MPa]
58 333.33

Table 3 presents the material parameters for the non-linear Mie-Grüneisen EOS defined in LS-DYNA using the ***EOS_GRUNEISEN** keyword.

Table 3: Material parameters for Mie-Grüneisen EOS [17].

s [–]	Γ [–]	a [–]	c_0 [m/s]
1.40	1.97	0.48	5240

Additional material parameters required in the material model for AA6061-T6 are presented in Table 4.

Table 4: Additional material parameters for AA6061-T6 [16].

ρ [tonne/mm^3]	E [MPa]	ν [–]	C_p [N·mm/ tonne·K]	χ [–]	T_0 [K]	T_m [K]	C [–]	m [–]	α [K^{-1}]
$2.7\cdot10^{-9}$	70 000	0.33	$9.1\cdot10^{8}$	0.9	293	893	0.001	1	$2.32\cdot10^{-5}$

4 Numerical Modelling

The simulations in this study were conducted using LS-DYNA [18] (version R12.0.0). The simulations were run on a Linux cluster utilizing 16 cores per simulation and the computational times ranged from 3 minutes to 22 hours, depending on the problem at hand. Numerical models were established to reproduce the Piekutowski experiments, and to test the method on dual-layered Whipple shields. The primary focus of this study was on the coupled FEM/DES method.

4.1 Coupled finite element-discrete particle method (FEM/DES)

The FEM/DES model for the Piekutowski configuration with $t/D = 0.102$ is shown in Figure 2 from the side and front, as well as a cross-section view of the projectile. When using the coupled FEM/DES method in LS-DYNA, the target and projectile are initially modelled with solid elements. The conversion from solid elements to discrete particles is achieved through the keyword ***DEFINE_ADAPTIVE_SOLID_TO_DES.** The keyword adaptively transforms a Lagrangian solid part or part set to discrete element spheres (DES) when the Lagrangian solid elements comprising those parts fail. One (or more if desired) DES particles will be generated for each failed element as debris. The DES particles replacing the failed element inherit the properties of the failed solid element, including mass and kinematic state [19]. The properties of the DES particles are defined in the ***CONTROL_DISCRETE_ELEMENT** keyword. The targets in the Piekutowski studies were modelled with a mesh size of approximately 0.25 mm for all configurations, and the number of elements over the target thickness increased in accordance with the increased t/D ratio. The number of elements in the target ranged from 26 569 with $t/D = 0.026$ to 399 424 with $t/D = 0.424$. Due to the non-uniform mesh size inside the projectile, the mesh density was higher for the projectile than for the target. It was found that the mesh size in the outer layer of the projectile had to be roughly the same as the target mesh size. The mesh size in the projectile with a diameter of 9.53 mm varied from 0.1 mm in the centre to 0.35 mm in the outer layer, leading to a total of 137 781 elements. A boundary condition restricting nodal translation in the impacting direction was added to the front-facing outer edge of the targets to recreate the boundary conditions from the Piekutowski experiments. Contact was modelled with ***CONTACT_ERODING_SINGLE_SURFACE** for element-to-element contact and ***CONTACT_ERODING_NODES_TO_SURFACE** for particle-to-element contact. A contact friction coefficient μ = 0.01 was applied.

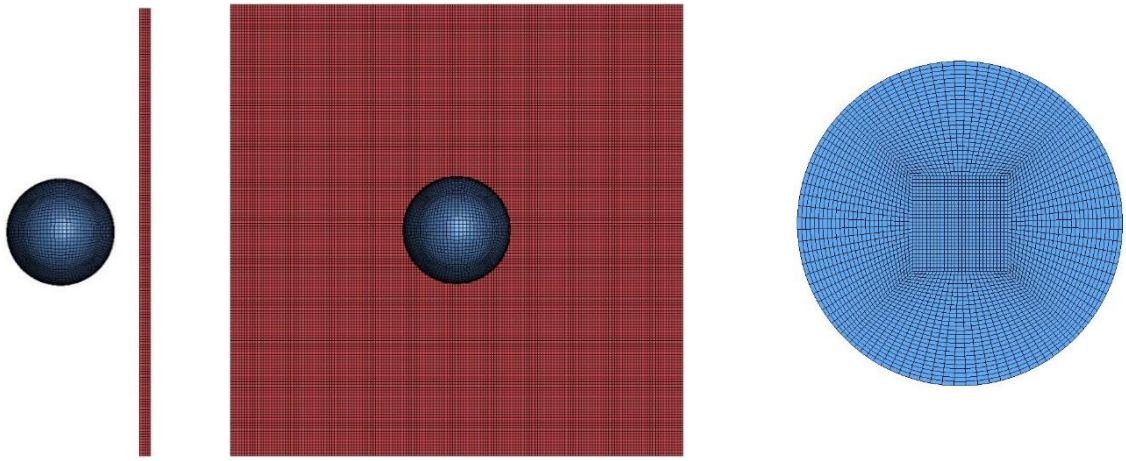

Fig.2: FEM/DES model of Piekutowski configuration with t/D 0.102. Side view (left), front view (centre) and cross-section of projectile (right).

4.2 Smoothed particle hydrodynamics (SPH)

The SPH models were generated with the same dimensions as the FEM/DES models and with the number of particles corresponding to the number of elements in the FEM/DES models. The SPH model was adapted from an LS-DYNA example model [20] and the properties of the SPH particles were defined in the ***CONTROL_SPH** keyword. The SPH models used the original Johnson-Cook constitutive model [11] and failure criterion [21], combined with a non-linear Mie-Grüneisen EOS. The contact was assumed to be frictionless in the SPH simulations.

5 Numerical Results with Piekutowski Experiments

5.1 FEM/DES method – numerical results

As shown in Figure 3 ($t/D = 0.084$), the numerical debris clouds consist of three components where the target particles make up the external debris cloud and the projectile particles and solid elements make up the internal structure.

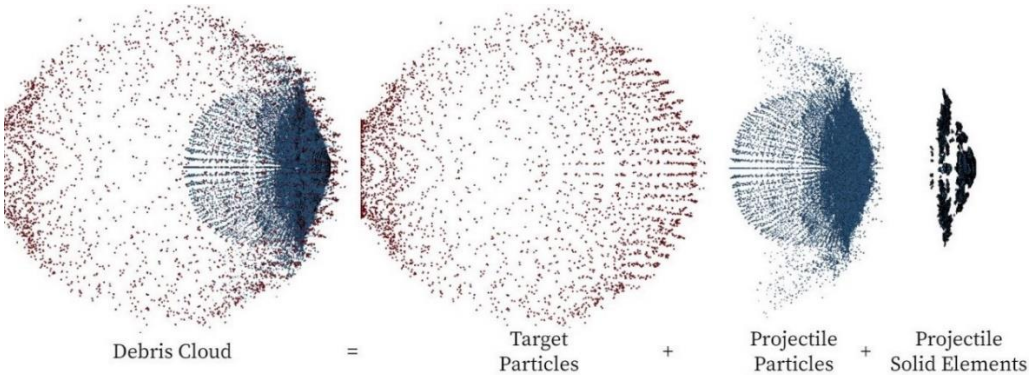

Fig.3: Components of numerical debris cloud, shown for t/D = 0.084.

Figure 4 shows some of the numerical results from Piekutowski's target thickness study for $t/D = 0.049$ and $t/D = 0.234$ with a linear and a non-linear EOS. The computational time ranged from 40 minutes with $t/D = 0.026$ to 5 hours with $t/D = 0.424$.

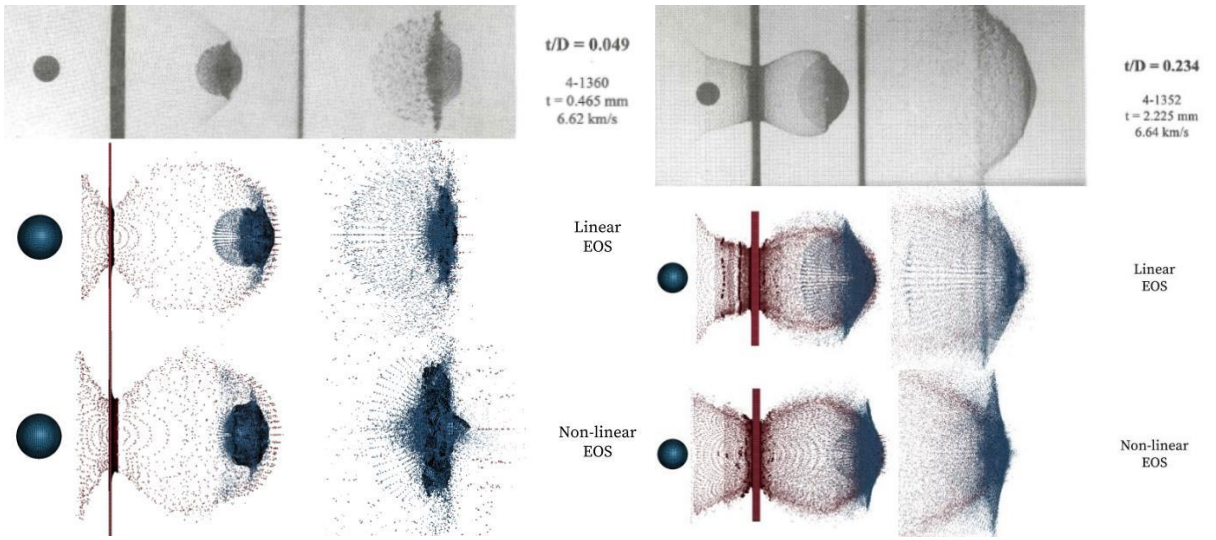

Fig.4: Numerical results from the target thickness study with t/D = 0.049 and 0.234 using the FEM/DES method with a linear versus a non-linear EOS compared to Piekutowski's experiments [10].

There is good agreement between the numerical results and the experimental results for the target thickness study. The linear EOS generally gives a spherical internal structure of the debris cloud, while the non-linear EOS gives an oval internal structure.

In addition to the visual comparison, debris cloud measurements were taken to evaluate the numerical results. The percentage of solid material of the debris clouds and the debris cloud diameter, as a function of t/D ratio, are shown in Figure 5. The percentage of solid material in the debris cloud describes the conversion from solid elements to particles and gives an understanding of the method's ability to describe phase changes and distribution of solid and molten/vapourised material in the debris cloud. The percentage of solid elements in the cloud decreases rapidly with increasing t/D ratio, and more than 95 percent of the projectile has been converted to particles after the impact for t/D ratios above 0.1. The debris cloud diameter measures the outer diameter of the disc of projectile particles located at the front of the debris cloud. The FEM/DES method produces a debris cloud with a smaller diameter than the experimental results, and the linear EOS is closer to the experimental results for most of the t/D ratios.

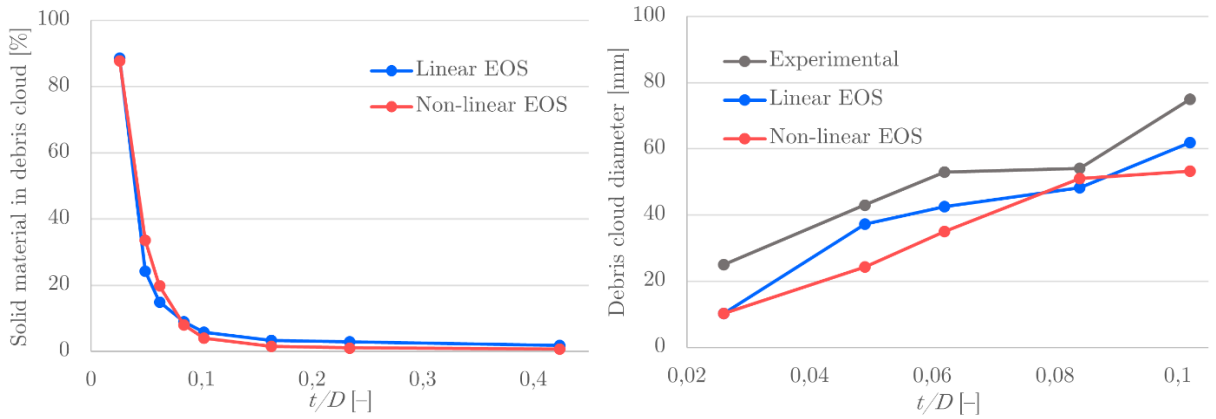

Fig.5: Percentage of solid material in debris clouds (left) and debris cloud diameter (right) with FEM/DES method as a function of t/D.

The residual velocity of the debris clouds is shown in Figure 6. The residual velocity of the debris cloud is a useful parameter when comparing the numerical and experimental results, because of the key role it plays in describing the momentum and kinetic energy of the fragments in the cloud and the damage they can cause to spacecraft. The residual velocity decreases with increasing t/D ratio for both linear and non-linear EOS, but the results with a linear EOS are significantly closer to the experimental results than with a non-linear EOS, and the difference increases with increasing t/D ratio.

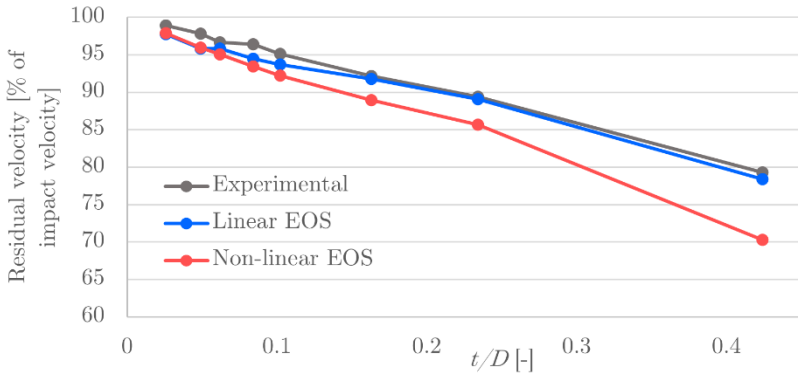

Fig.6: Residual velocity of debris clouds with FEM/DES method as a function of t/D.

5.2 SPH method – numerical results

The numerical results from Piekutowski's target thickness study using the SPH method are presented below and compared to the experimental results and the FEM/DES method. Figure 7 shows the results for $t/D = 0.102$ and $t/D = 0.424$. The computational time with the SPH method ranged from 3 minutes with $t/D = 0.026$ to 25 minutes with $t/D = 0.424$.

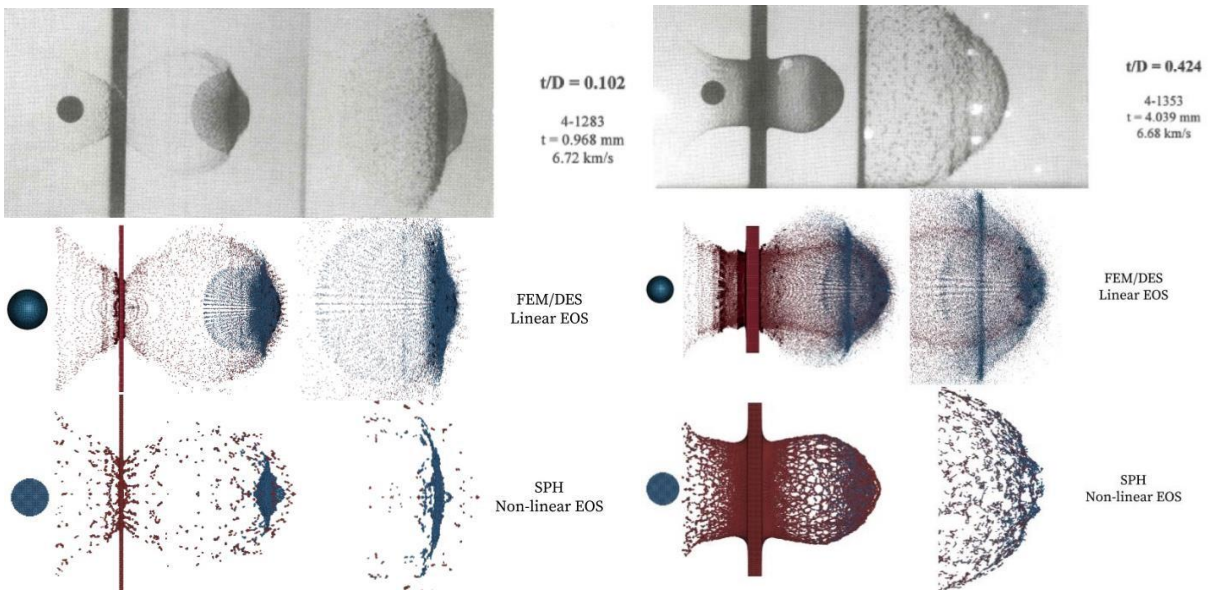

Fig.7: Numerical results from the target thickness study with t/D = 0.102 and 0.424 using the FEM/DES and SPH method, compared to Piekutowski's experiments [10].

As shown in Figure 7, the SPH method does not produce a spherical internal structure in the debris cloud when $t/D = 0.102$. Instead, all the projectile material is distributed along the front of the cloud. At $t/D = 0.424$, the SPH method is visually more alike the experimental results than the FEM/DES method.

Figure 8 shows the residual velocity of the debris clouds as a function of the t/D ratio for the SPH and FEM/DES method, compared to the experimental results. The measurements show that the SPH results differ significantly from the experimental results and the FEM/DES results. The residual velocity is underestimated in the SPH results, and the difference from the experimental results increases with the t/D ratio.

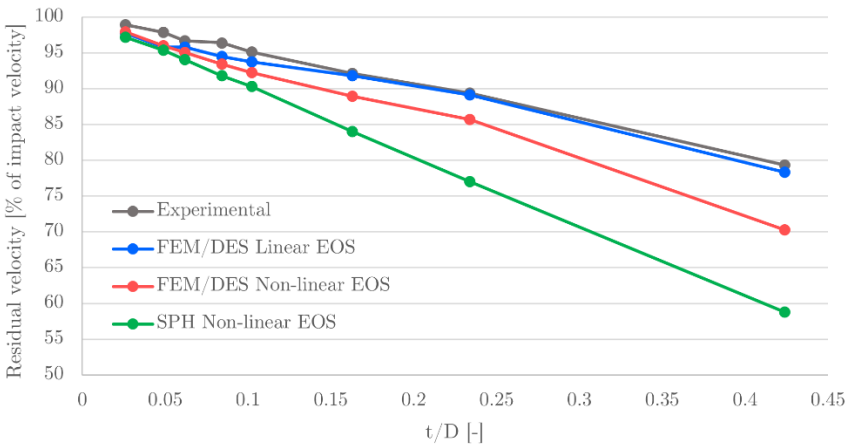

Fig.8: Residual velocity of the debris clouds from the FEM/DES method with a linear and a non-linear EOS, the SPH method, and experimental data, as a function of the t/D ratio.

6 FEM/DES method applied to Whipple Shields

Numerical models of the dual-wall Whipple shield in aluminium alloy AA6061-T6 presented by Christiansen [22] were created with the FEM/DES method using a linear EOS in order to assess the method's ability to accurately model the resulting damage when the debris cloud impacts a structure. The Whipple shield consisted of a 1.2 mm thick bumper, followed by a 100 mm standoff distance, and a 3.2 mm thick rear wall. Failure of the shield was defined as perforation or spalling from the rear wall.

The numerical result from the dual-wall Whipple shield impacted by a projectile with a diameter of 5.2 mm at 8 km/s is shown in Figure 9 at four points in time. Here, the impact velocity falls within the hypervelocity regime, and the projectile is expected to be fully converted to particles that impact the rear wall in a similar manner as a blast load, leading to mostly global deformations.

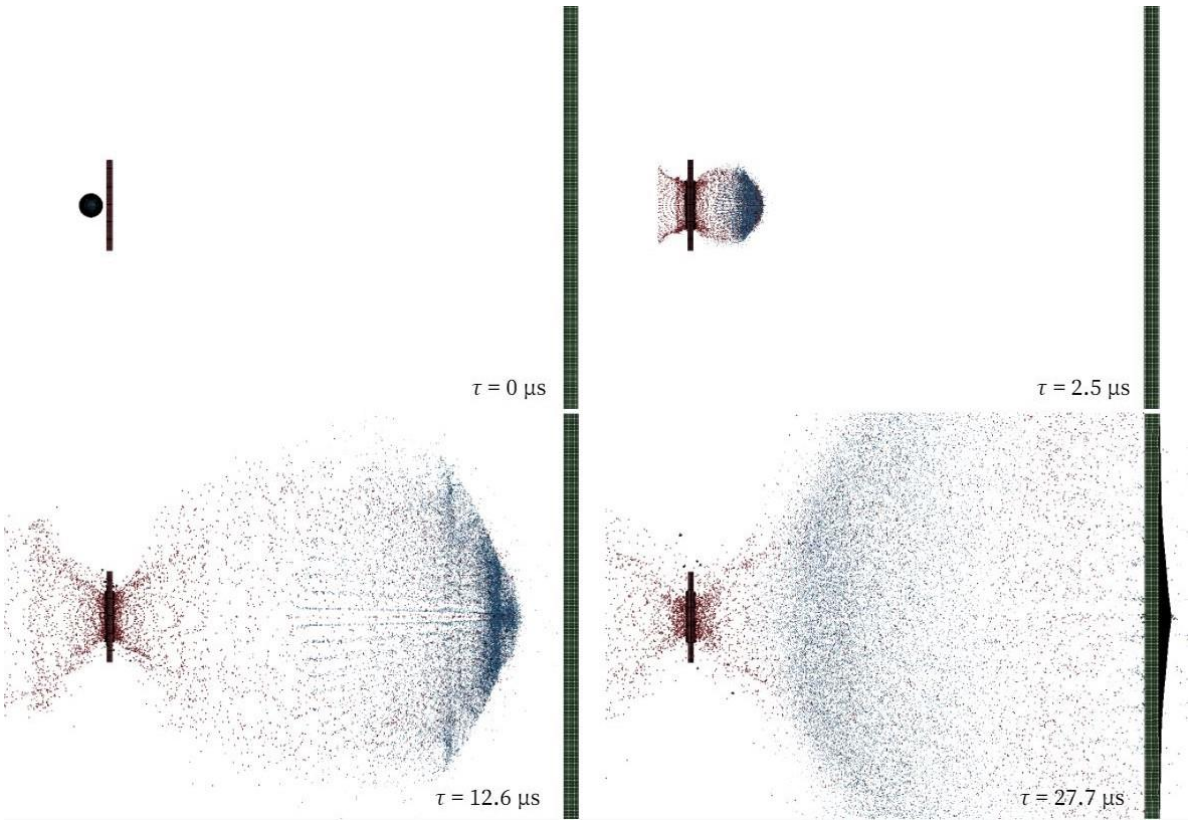

Fig.9: Whipple shield impacted at 8 km/s by a projectile with 5.2 mm diameter.

The debris cloud in Figure 9 can be seen fully converted to particles at τ = 2.5 µs and 12.6 µs, with a higher density of particles near the centre of the cloud. The cloud expands radially as it moves across the standoff distance and impacts the rear wall over a wide area, leading to spalling on the rear side of the rear wall. Global deformation of the rear wall can be seen around the spalling point. The majority of the particles are reflected back towards the bumper.

7 Conclusions

Hypervelocity impacts were modelled in LS-DYNA using a coupled finite element-discrete particle method (FEM/DES), and the results were compared to experimental data from the literature and the SPH method. Impacts from orbital debris by projectiles with diameter below 1 cm were considered, and AA6061-T6 was assumed for both the target and the projectile material (as in the experimental tests). The numerical results showed that the FEM/DES method can reproduce the experimental debris clouds from the literature and found that the results with a linear EOS were closer to the experimental data than those with a non-linear Mie-Grüneisen EOS. The debris cloud simulations were repeated with the SPH method, and it was found that the FEM/DES method results were closer to the experimental results than the results using the SPH method. The FEM/DES method was applied to a dual-wall Whipple shield configuration and was able to accurately capture the damage from the debris cloud on the rear wall. The results obtained with the FEM/DES method in this study are promising, and the method should be validated and compared to a larger set of experimental impact data, particularly experimental data with Whipple shields and other target materials.

Acknowledgements

The present work has been carried out with financial support from the Centre of Advanced Structural Analysis (CASA), Centre for Research-based Innovation, at the Norwegian University of Science and Technology (NTNU) and the Research Council of Norway through project no. 237885 (CASA).

Literature

[1] F. L. Whipple, “Meteorites and Space Travel,” *Astron. J.*, no. 52:131, 1947.
[2] E. L. Christiansen, K. Nagy, D. M. Lear, and T. G. Prior, “Space station MMOD shielding,” *Acta Astronaut.*, vol. 65, no. 7–8, pp. 921–929, 2009, doi: 10.1016/j.actaastro.2008.01.046.
[3] F. Plassard, J. Mespoulet, and P. Hereil, “Hypervelocity impact of aluminium sphere against aluminium plate : experiment and LS-DYNA correlation,” in *11th European LS-DYNA Conference*, 2017, pp. 1–11.
[4] E. Giannaros, A. Kotzakolios, S. Tsantzalis, V. Kostopoulos, and G. Campoli, “Novel simulation of composite material behavior subjected to hyper-velocity impact (HVI) and produced secondary debris by using smoothed- particle hydrodynamics code (SPH) methodology in,” 2017.
[5] D. Lacerda and J. Lacome, “Simulations of Hypervelocity Impacts with Smoothed Particle Hydrodynamics,” 2001.
[6] T. Legaud, M. L. E. Garrec, N. Dorsselaer, and V. Lapoujade, “Improvement of satellites shielding under high velocity impact using advanced SPH method,” 2019.
[7] F. Plassard, H. Abdulhamid, P. Deconinck, P. Héreil, and C. Puillet, “Experimental and Numerical Study of Submillimeter- Sized Hypervelocity Impacts on Honeycomb Sandwich Structures,” 2019.
[8] M. H. Farahani and N. Amanifard, “A High-Velocity Impact Simulation Using SPH-Projection Method,” *IJE Trans. A Basics*, vol. 22, no. 4, pp. 359–368, 2009.
[9] T. Børvik, S. Dey, L. Olovsson, and M. Langseth, “Impact of APM2 bullets on AA6082-T4 aluminium plates,” in *Proceedings of the 11th Hypervelocity Impact Symposium*, p. (p.13).
[10] A. J. Piekutowski, “Formation and Description of Debris Clouds Produced by Hypervelocity Impact,” 1996.
[11] G. R. Johnson and W. H. Cook, “A constitutive model and data for metals subjected to large strains, high strain rates and high temperatures,” in *Proceedings of the 7th International Symposium on Ballistics*, 1983, pp. 541–547.
[12] T. Børvik, O. S. Hopperstad, T. Berstad, and M. Langseth, “A computational model of viscoplasticity and ductile damage for impact and penetration,” *Eur. J. Mech. A/Solids*, vol. 20, no. 5, pp. 685–712, 2001, doi: 10.1016/S0997-7538(01)01157-3.
[13] M. Scapin, “Shock-wave and high strain-rate phenomena in matter-modeling and applications,” Politecnico di Torino, 2013.
[14] M. G. Cockroft and D. J. Latham, “Ductility and workability of metals,” *J. Inst. Met.*, vol. 96, pp. 33–39, 1968.
[15] R. M. Færgestad, “Modelling and simulation of hypervelocity impact against debris shields for spacecraft protection,” Norwegan University of Science and Technology, Department of Structural Engineering, Structural Impact Laboratory (SIMLab), 2021.
[16] H. N. G. Wadley *et al.*, “Deformation and fracture of impulsively loaded sandwich panels,” *J. Mech. Phys. Solids*, vol. 61, no. 2, pp. 674–699, 2013, doi: 10.1016/j.jmps.2012.07.007.

[17] D. Steinberg, *Equation of State and Strength Properties of Selected Materials*, UCRL-MA-10. Livermore, CA, United States: Lawrence Livwermore National Laboratory, 1996.
[18] Livermore Software Technology (LST), “LS-DYNA, https://www.lstc.com/products/ls-dyna [accessed 30.05.2021].” .
[19] Livermore Software Technology (LST), *LS-DYNA R12 Keyword User’s Manual*, vol. I. 2020.
[20] Livermore Software Technology (LST), “LS-DYNA Examples - SPH - Sieve, https://www.dynaexamples.com/sph/sieve [accessed 15.03.2021].”
[21] G. R. Johnson and W. H. Cook, “Fracture characteristics of three metals subjected to various strains, strain rates, temperatures and pressures,” *Eng. Fract. Mech.*, vol. 21, no. 1, pp. 31–48, 1985, doi: 10.1016/0013-7944(85)90052-9.
[22] E. L. Christiansen, “Handbook for Designing MMOD Protection,” 2009.